Geophysical Journal International

Geophys. J. Int. (2017) **209,** 1080–1094 doi: 10.1093/gji/ggx077
Advance Access publication 2017 February 24
GJI Geomagnetism, rock magnetism and palaeomagnetism

Two types of impact melts with contrasting magnetic mineralogy from Jänisjärvi impact structure, Russian Karelia

Elena S. Sergienko, Andrei Kosterov and Petr V. Kharitonskii

St. Petersburg State University, St. Petersburg 199034*, Russia. E-mail:* *e.sergienko@spbu.ru*

Accepted 2017 February 23. Received 2017 February 22; in original form 2016 August 3

SUMMARY

Palaeomagnetic and rock magnetic studies of impact-related rocks can provide important constraints for deciphering geophysical records from suspected impact structures, their geochronology, and, in the case of very large impacts, their effect on the Earth as a whole. However, the palaeomagnetic record in impact-related rocks may be ambiguous because of the uncertain origin of their natural remanent magnetization (NRM). Towards this end, we carried out a comprehensive rock magnetic and mineralogical study of tagamites (impact melts) from the Jänisjärvi astrobleme, Russian Karelia. Chemical composition of magnetic minerals and non-magnetic matrix was evaluated by scanning electron microscopy (SEM) and X-ray analysis. Magnetic minerals were identified using thermomagnetic analysis at high and low temperatures, whereas their domain state was evaluated from hysteresis measurements and magnetic force microscopy. Jänisjärvi tagamites appear to belong to two essentially different types arising from the differences in the impact melt crystallization conditions. Type I tagamites were likely formed by an extremely rapid cooling of a superhot melt with initial temperatures well above 2000 °C. Type II tagamites originate from cooler and more iron-enriched melt. Common to the two types is that they both contain a substantial amount of fine inclusions in silicate matrix tens of nanometres to few micrometres in size, which appear to be a major, in some cases dominant, magnetic mineral carrying a significant part of rocks NRM. Structurally, these inclusions are heterogeneous objects consisting of two phases showing both chemical and magnetic contrast.

Key words: Magnetic properties; Microstructure; Rock and mineral magnetism; Impact phenomena.

1 INTRODUCTION

Impact craters (astroblemes) are formed as a result of collision of small cosmic bodies with planetary surfaces. As such, they are characterized by a peculiar internal structure and rock composition. Through the geological past, impacts played a significant role in the formation of terrestrial planets' surfaces and their subsequent evolution. Study of impact structures may yield valuable information in meteoritics, planetary physics and evolution of the Solar System, as well as in physics of explosive impact processes. Of many methods applied to study terrestrial impact structures, palaeomagnetism and rock magnetism have proved useful to estimate the age of the impact structures (Elming & Bylund 1991; Schmidt & Williams 1991, 1996; Plado *et al.* 2000; Elmore & Dulin 2007), address the issues of lithology, stratigraphy, thermal regime of their formation and influence of impacts on regional geological settings (Pesonen *et al.* 1992; Plado *et al.* 2000; Riller 2005; Salminen *et al.* 2006; Halls 2009; Fairchild *et al.* 2016).

Collision of small cosmic bodies with the Earth's surface produces a range of impact-related rocks (impactites, for short) that are a product of the transformation of original igneous, sedimentary, or metamorphic rocks. Impactites are classified according to a degree of target rocks transformation, nature of occurrence, lithological type of fragments, chemical composition of impact melting products and their relative proportions (Dressler & Reimold 2001; Zhdanov *et al.* 2009). Three main classes of impactites are recognized: shock-metamorphosed target rocks and impact lithic breccias (containing 0–10 per cent of impact melt) and impactites *sensu stricto* that contain more than 10 per cent of melting products or consist entirely of the latter. Impactites are further divided into tectic-massive rocks that form during melt solidification (tagamites, named so after a typical locality at Tagamy Hills, Popigai impact structure and impact pumices and slags), and tektoklastic rocks where the impact glass is present as fragments and bombs (suevites).

Geologically, typical astroblemes are composed of several structural-lithological complexes: base (target rocks), allogenic breccia and impactites, filling (sedimentary rocks), ceiling (rock strata showing regional development and overlying the two above complexes) and injection (magmatic body intruding base and/or impact-related complexes, Masaitis *et al.* 1980; Dressler & Reimold 2001).

Regarding the applicability of the palaeomagnetic method to the studies of impact structures there are two conflicting opinions. On the one hand, it seems possible that the characteristic natural remanent magnetization (NRM) component dates from the time of impact event and may therefore be associated with it, as, for example, in Keurusselkä (Raiskila *et al.* 2011), Vredefort (Cloete *et al.* 1999; Gibson *et al.* 2001; Henkel & Reimold 2002; Carporzen *et al.* 2005), Acraman (Schmidt & Williams 1996), or Chicxulub (Steiner 1996; Pilkington *et al.* 2004) impact structures. On the other hand, it was suggested that the magnetization of impact-related rocks may not be synchronous with the impact itself, being the product of various physical and chemical processes (e.g. hydrothermal, typical of many large impact craters) during the later stages of rocks evolution. Such behaviour was reported, for example, for Lonar (Poornachandra Rao & Bhalla 1984; Louzada *et al.* 2008) and Manson (Steiner *et al.* 1996) structures. At the same time, magnetic properties of impact-related rocks are relatively little studied, and existing data are at best incomplete and/or controversial (Carporzen *et al.* 2005; Koch *et al.* 2012; Eitel *et al.* 2014, 2016; Hervé *et al.* 2015; Rochette *et al.* 2015).

Palaeomagnetism of Jänisjärvi impactites was previously studied by Salminen and coworkers (Salminen *et al.* 2006). All types of impact-produced lithologies were measured: tagamites, suevites and impact breccias. NRM was found to be carried mostly by multidomain (MD) titanomagnetite which the authors consider the primary, however hypothesizing also the presence of secondary titanomagnetite and ilmenohematite. Nevertheless, the palaeomagnetic pole position calculated from the direction of NRM characteristic component did not correspond to the age of the impact. The authors therefore concluded that isotopic geochronology methods may yield ambiguous results for impactites.

This study specifically concerns the magnetomineralogical composition of tagamites from Jänisjärvi astrobleme, a Late Precambrian impact structure exposed in Russian Karelia, 220 km northeast from St. Petersburg. Our major goal was to determine which magnetic mineral(s) carry characteristic components of NRM in impact rocks. For this purpose, we carried out microscopic and microprobe analysis, studied the magnetic properties, and constructed a theoretical model of the magnetic state of these rocks.

2 GEOLOGY AND SAMPLING

Jänisjärvi impact structure is located in Russian Karelia in the southeastern part of the Fennoscandian (Baltic) Shield, about 25 km north of Lake Ladoga (Fig. 1). In the modern landscape, it appears as a nearly circular lake about 14 km in diameter, clearly different in shape from nearby lakes of glacial origin. The impact origin for the Jänisjärvi structure was first proposed on the basis of its orography and geophysical fields (Dence 1971); later, it was confirmed by finding of diaplectic minerals and shatter cones (Masaitis *et al.* 1976). Age of Jänisjärvi structure determined with the $^{40}Ar/^{39}Ar$ method is 682 ± 4 Ma (Jourdan *et al.* 2008). In the gravity data, the structure has a diameter of about 16 km (Elo *et al.* 2000).

Geological structure of the area around Jänisjärvi impact structure and sampling sites are shown in Fig. 2 (Fel'dman *et al.* 1982). The base complex is composed of interbedded quartz-sericite-biotite, quartz-biotite and biotite-quartz schists with porphyroblasts of staurolite, andalusite, garnet and cordierite which belong to the

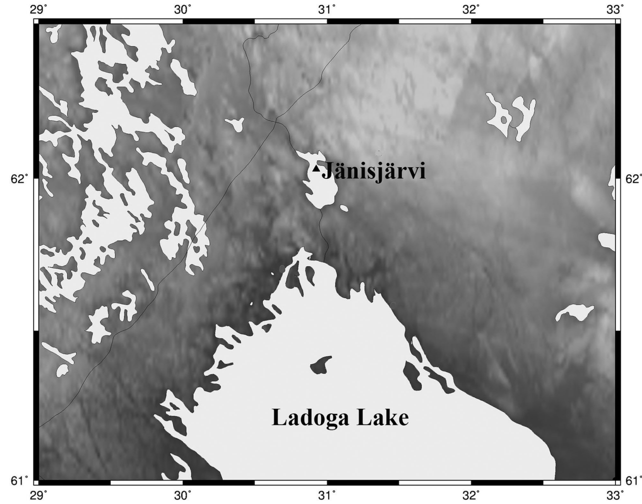

Figure 1. The geographical position of the Jänisjärvi impact structure.

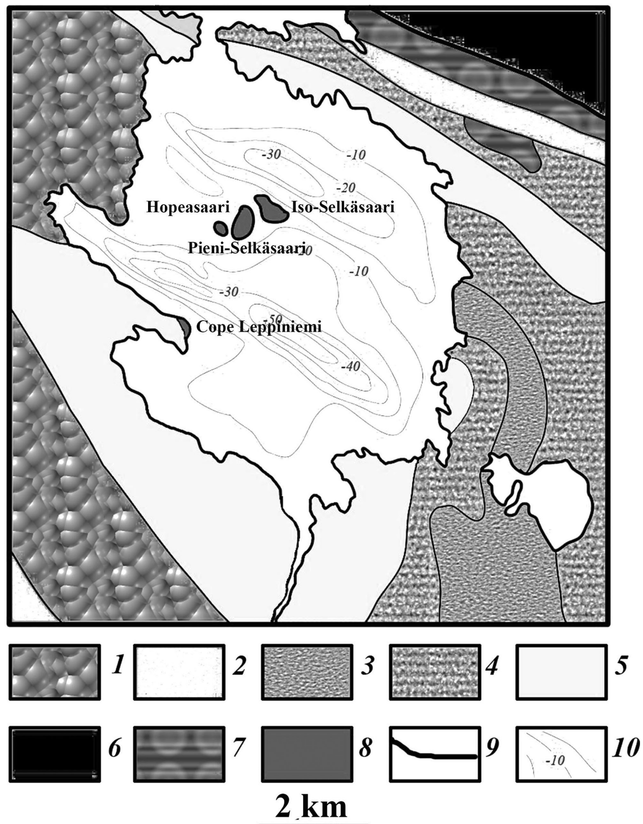

Figure 2. Schematic geological map of the Jänisjärvi astrobleme area: 1—Pälkjärvi formation; 2–5—Naatselkä formation (2—undivided, 3—lower, 4—middle and 5—upper); 6—Early-Middle Proterozoic rocks; 7—gabbro-diabase; 8—impactites; 9—faults and 10—isobaths of the Jänisjärvi Lake.

Ladoga series (Naatselkä and Pälkärvi suites). The age of target rocks is estimated as 1885 ± 30 Ma (Masaitis *et al.* 1980).

Impactites are presented by tagamites, suevites lying hypsometrically below tagamites, and allogenic breccia. Tagamites are only exposed at Cape Leppiniemi and at three islands in the central part of the lake—Hopesaari (HS), Pieni-Selkäsaari and Iso-Selkäsaari (IS), the latter being the closest to the geometrical centre of the astrobleme. 80–100 per cent of tagamites by volume is a fine-grained crystalline mass with aphanic amygdaloidal texture, containing up to 20 per cent of the debris schists and minerals. The rocks contain relict minerals, such as quartz, staurolite, graphite and garnet. Impact-formed minerals make up to 80 per cent of rock volume and are represented by plagioclase, dusted by ore minerals throughout, cordierite, enstatite (orthopyroxene of variable composition) and ilmenite. Secondary biotite, chlorite and magnetite (titanomagnetite) develop over minerals formed by impact, most often enstatite.

Outcrops of tagamites selected for this study are located along the coastlines in the southern and southwestern parts of islands Hopesaari (HS) and Iso-Selkäsaari (IS). Sampling was carried out so that the entire profile forms a continuous line on each of the islands, samples being numbered HS01 to HS16 and IS01 to IS16, respectively. On both islands, the length of a sampling profile was 100–200 m, and the distance between the two profiles amounted to ~2500 m. Thus, it was possible to track changes in the magnetic and structural properties of tagamites along the total of about 300 m from the astrobleme centre to the periphery (IS16→ HS01).

3 METHODS

Samples for microscopic study were prepared as polished sections. Fragments of approximately 10 × 10 mm were fixed in an epoxy resin to form a 1″ diameter mounting cup using a vacuum impregnation unit StruersCitoVac. The surface was then ground and polished using a semi-automatic machine Buehler Minimet 1000. Individual mineral grains and their clusters were first observed with a digital microscope Leica DVM5000 and a polarization microscope Leica DM 4500P. Backscattered electron images were collected and analysis of the chemical composition of the magnetic minerals was performed using a Hitachi S-3400 N SEM with a wavelength dispersive spectrometer WDS-INCA 500, a field emission cathode SEM Zeiss Merlin and a QUANTA System 200 3-D with an analytic complex Pegasus 4000. Since the effective diameter of the electron probe is about 2 μm, to study smaller grains, a distribution of chemical elements, specifically Fe, O, Si, Al, Mg and Ti, were mapped over typical areas of about 75 × 50 μm^2. The distribution of magnetic fields over the surface of the sample was visualized by magnetic force microscopy using an atomic force microscope INTEGRA-AURA (NT-MDT, Russia) with a CoCr magnetic probe.

Study of magnetic properties included measuring temperature dependences of low-field magnetic susceptibility and of hysteresis loops and backfield magnetization curves at room temperature. Susceptibility versus temperature curves were measured between −192 and 700 °C using a susceptibility bridge MFK1-FA (AGICO). The sample was first cooled to liquid nitrogen temperature, and a susceptibility curve during warming to room temperature was traced. Then, the susceptibility was measured on heating and cooling the sample from room temperature to 700 °C and back in argon atmosphere. Finally, a second low-temperature susceptibility curve has been measured. Curie temperatures have been determined as a derivative of the respective susceptibility curves. Curves measured at low temperatures were primarily employed to trace mineralogical alteration induced by heating. Besides, observation of a characteristic peak associated with the Verwey transition might help to infer presence or absence of magnetite in our samples. Hysteresis loops have been measured in a maximum field 2 T using a LakeShore Cryotronics 7410 vibrating sample magnetometer. The same instrument was used to trace isothermal magnetization curves and backfield demagnetization curves. For representative samples, first-order reversal curves (FORC) were measured with a Princeton Measurements Corporation 3900 VSM instrument at Institute of Physics of the Earth, RAS (Moscow). Generally, between 170 and 280 FORCs have been measured for each sample, in order to ensure that field increments were roughly of the order of bulk coercive field divided by a factor of ten. FORC distributions have been computed with the VARIFORC v.2.03 software (Egli 2013). For the same specimens, hysteresis loops in a 1.5 T maximum field, IRM and backfield curves were also collected.

For the selected samples, the magnetic mineralogy was characterized using low-temperature measurements with an MPMS 3 instrument (Quantum Design). Saturation isothermal remanent magnetization (SIRM) acquired in a 5 T field at 1.8 K after cooling either in zero (ZFC) or in a 5 T (FC) magnetic field was traced during warming in a zero field. Similarly, SIRM (5 T) acquired at 300 K was traced in a zero field on cooling to 1.8 K and warming back to 300 K. All data were collected in the MPMS 3 temperature sweeping mode at 2 K min^{-1}, recording about 20 magnetization measurements per Kelvin. For the samples used for the above measurements, hysteresis loops in the 7 T maximum field and backfield curves were also traced with the MPMS 3 instrument at 295 K.

4 RESULTS

4.1 Microscopic observations

Microscopic examination of polished sections shows that tagamites can be classified into two varieties which differ by grain size and number of inclusions in the rock (non-magnetic) matrix. The first variety (type I thereafter) contains a large amount of debris and is characterized by broadly distributed, generally rather coarse grain size. In the second variety (type II), grains are relatively uniform and much finer.

Microscopy and microprobe analysis reveal several iron-bearing mineral phases (Fig. 3). Iron sulphides are represented by large, >100 μm, grains of chalcopyrite often bordered by an iron oxide film. Fine irregular shaped grains of pyrite are also observed developing over biotite. Ilmenite, characterized by oxide compositions TiO_2—51.9 per cent, FeO—43.0 per cent, with minor Mn and Mg, occurs as large, up to 100 μm anhedral, columnar, needle-shaped grains and clusters thereof. Some rutile is also present. Homogeneous iron-titanium oxide grains 5–10 μm in size are characterized by a relatively high TiO_2 content, minor Mn, Cr, Ca and Al). Such grains however occur only in the type II tagamites, and even there they are quite rare. The non-magnetic matrix is mostly plagioclase. On the basis of the anorthite content it can be classified as labradorite for type II tagamites (59 per cent anorthite on average) and as oligoclase for type I tagamites (23 per cent anorthite on average).

Fine inclusions of ore minerals (referred to as ‘ore dust’ by Masaitis *et al.* 1980) occur as clusters of < 2 μm grains developing over plagioclase. In the type I tagamites, they are observed as grains uniformly scattered over large, up to hundreds of micrometres, plagioclase crystals (Fig. 3g). In the type II tagamites, where plagioclase crystals are much smaller (<30 μm), fine inclusions are localized within separate, clearly defined clusters 10–20 μm in size (Figs 3e and f). Volumetric concentration of fine inclusions within a cluster is generally several percent, reaching in some cases 10 per cent.

Morphologically, fine inclusions appear to be small inhomogeneous two-phase grains (from <100 nm to 2 μm, Fig. 4), consisting of a smaller bright area and a larger dark area. We attempted to investigate chemical composition of individual inclusions with microprobe analysis (Fig. 5). However, since at accelerating voltage of 20 kV the effective diameter of the probe is about 2 μm, which

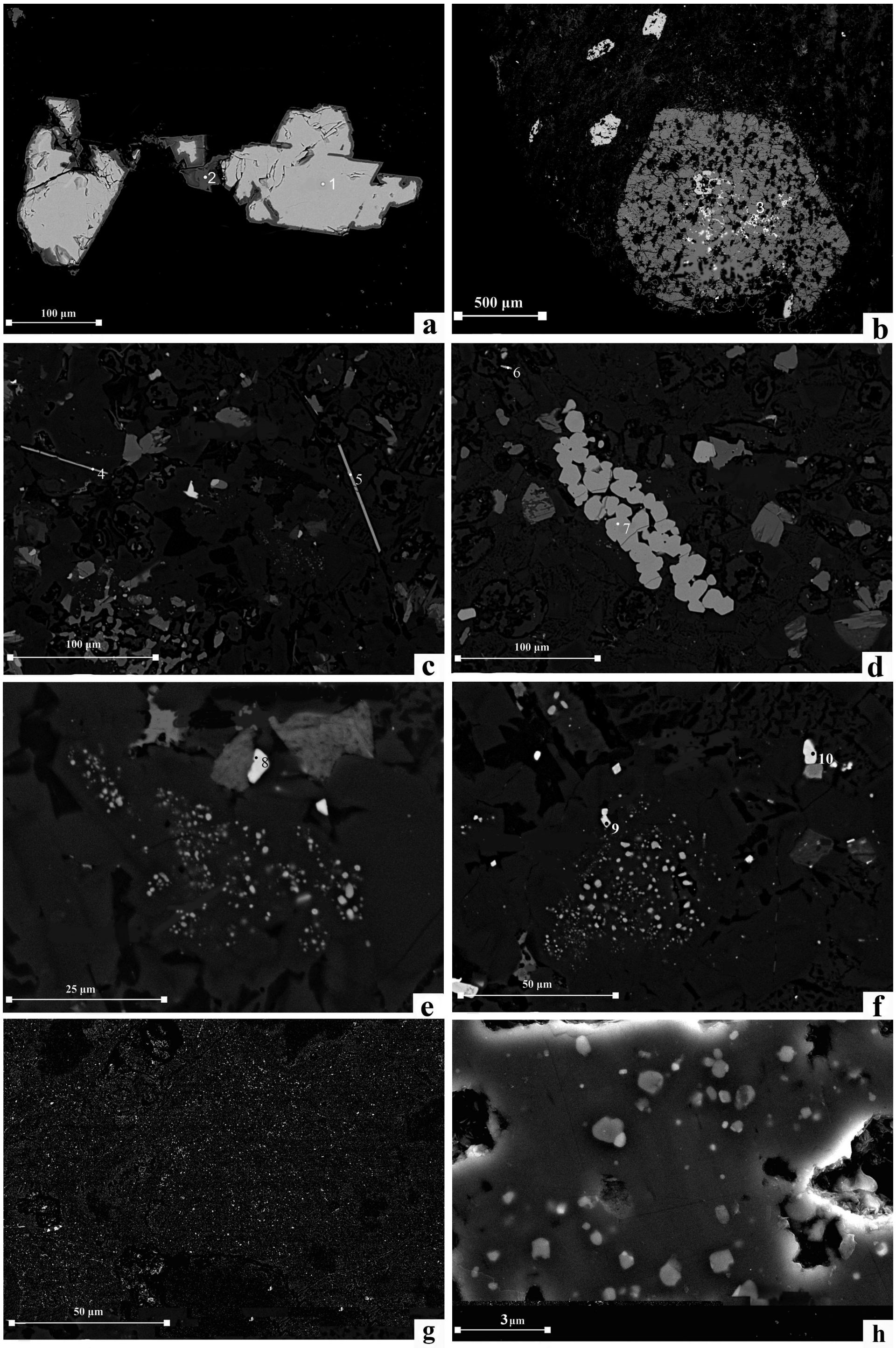

Figure 3. Photomicrographs of ore minerals in tagamites from the Jänisjärvi impact structure with the microanalysis results at points numbered 1–10. (a) chalcopyrite bordered by a film of iron oxide (1: S (35.1) Fe (30.9) Cu (34.0) wt%); 2: Fe (51.4) O (37.4) wt%), (b) fine exsolution of pyrite (3: S (52.7) Fe (47.3) wt%) in biotite, (c) and (d) ilmenite grains (4: O (39.4) Ti (22.1) Fe (25.5) wt%; 5: O (34.2) Ti (28.6) Fe (32.4) wt%; 6: O (31.2) Ti (32.5) Fe (35.8) wt%; 7: O (42.1) Ti (21.4) Fe (24.9) wt%) of various shape;(e) and (f) grains of iron-titanium oxides (8: O (32.9) Ti (14.4) Fe (38.3) wt%; 9: O (33.3) Ti (12.8) Fe (35.3) wt%; 10: O (31.2) Ti (16.8) Fe (44.0) wt%) and fine inclusions in type II tagamites, (g) fine inclusions in a plagioclase grain in type I tagamites and (h) individual two-phase grains of fine inclusions.

is larger or close to the size of studied grains, the values of absolute elemental composition are not very informative. Use of lower voltages while reducing the probe size would not provide complete data on heavy elements, particularly on iron. We therefore compared chemical composition of the matrix (point 3 in Fig. 5a), and of the bright and the dark part of an individual grain belonging to a fine inclusions cluster (points 1 and 2 in Fig. 5a, respectively). The results are shown in Fig. 5(b).

The inclusion grain appears greatly enriched in iron compared to the matrix and contains impurities of magnesium, aluminum,

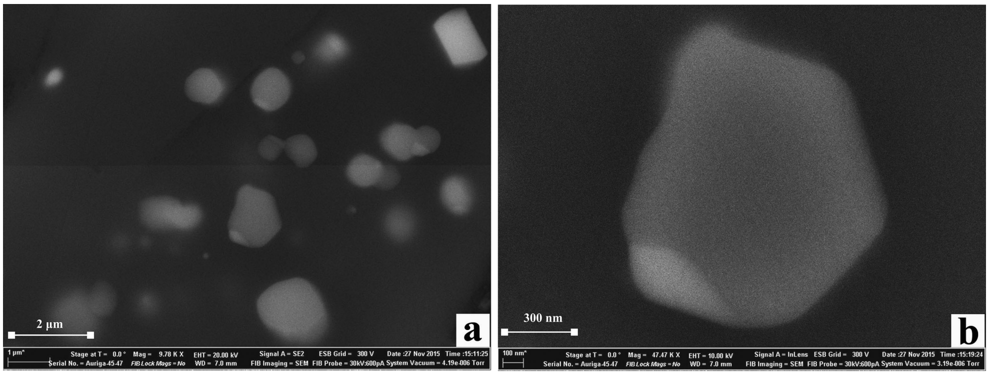

Figure 4. Close-up photomicrographs of fine inclusions in tagamites.

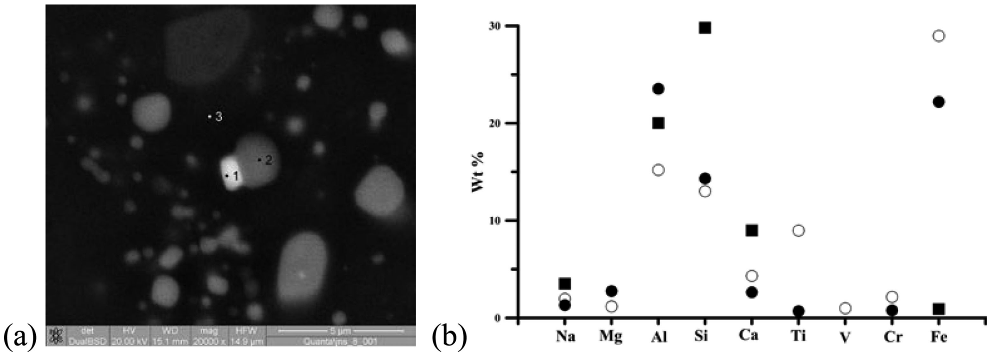

Figure 5. (a) Photomicrograph of fine inclusions, indicating microanalysis points and (b) diagram comparing the content of chemical elements in the light (1, open circles in the diagram), and dark (2, solid circles) areas of an inclusion and in the non-magnetic matrix (3, square).

titanium and chromium. Also, the dark part of the grain is enriched in aluminum compared to the matrix and light part of the grain. Titanium content is relatively low, up to 10 per cent even in more Ti-rich areas (bright) while it is nearly zero in dark areas. Grains in fine inclusions clusters can therefore be considered as a two-phase system 'Al, Ti-bearing magnetite—Al, Mg-bearing magnetite' with different content of impurity elements.

To further constrain the chemical composition of fine inclusions, we mapped the area distributions of selected elements for the two types of tagamites (Figs 6 and 7, respectively). These data confirm that inclusions are enriched in aluminum and magnesium compared to the rock matrix. However, the Ti distribution over the area shown in Fig. 5 does not show distinct anomalies. This would suggest that one (minor) phase in this and similar grains could be magnetite, containing in some cases a small amount of titanium, and the second (major) phase—magnetite with significant amount of aluminum and magnesium impurities.

To find out whether fine inclusions are magnetic, and may therefore contribute to samples magnetic properties, a representative selection of these grains was investigated with magnetic force microscopy. Atomic force images (Figs 8a–c) show that the respective grains stand above the generally flat relief of the rock matrix. Distributions of stray magnetic fields (Figs 8b–d) though suffering from instrumental artefacts (horizontal stripes in Fig. 8b and crisscrossing highs and lows with about 1 μm period in both figures) nevertheless indicate that both grains yield a strong magnetic signal and can therefore be considered as ferrimagnetic. Signals from the two grains shown in Fig. 8(b) resemble a characteristic appearance of force lines from magnetic dipoles magnetized perpendicularly to the viewing plane, so that the magnetic moment of the upper right grain is directed outward and that of the lower left grain inward. The grain in Fig. 8(d) shows a more complicated magnetic structure with the outer part yielding the strongest magnetic contrast.

4.2 Bulk magnetic properties

Two types of tagamites show different magnetic properties as well. In the type I tagamites both NRM and low-field magnetic susceptibility (Table 1) are low, ranging from < 1 mA m^{-1} to about 50 mA m^{-1} and 2×10^{-4} to 4.8×10^{-4} SI units, respectively. The single outlier sample, IS14 (see below) yields somewhat higher susceptibility, about 1×10^{-3} SI units while having the NRM value well within the above range for type I samples. In the type II tagamites NRM and low-field susceptibility are considerably higher and show larger variance than in type I, ranging from 20 mA m^{-1} to about 400 mA m^{-1} and 4.4×10^{-4} to 6×10^{-3} SI units, respectively.

Thermomagnetic behaviour of the studied rocks is quite variable, particularly for type I samples (Figs 9a and b). In these latter it depends primarily on the content of a strongly magnetic phase. The only sample from this group, where a strongly magnetic phase dominates, IS14, shows almost reversible k–T curve with the highest Curie temperature for the whole collection (560 °C). Its low-temperature curve shows faint but visible shoulder around −150 °C which may be associated with the Verwey transition. On the contrary, sample IS08 (Fig. 9b) shows nearly paramagnetic behaviour until magnetomineralogical changes apparently forming a magnetite-like phase start at about 500 °C.

For most type II samples (Figs 9c–e), low-temperature susceptibility curves combine, in different proportions, two principal behaviours, namely, monotonous decrease and similarly monotonous increase with temperature. In few samples, a relatively minor peak or shoulder at 110–115 K which may be a signature of the Verwey

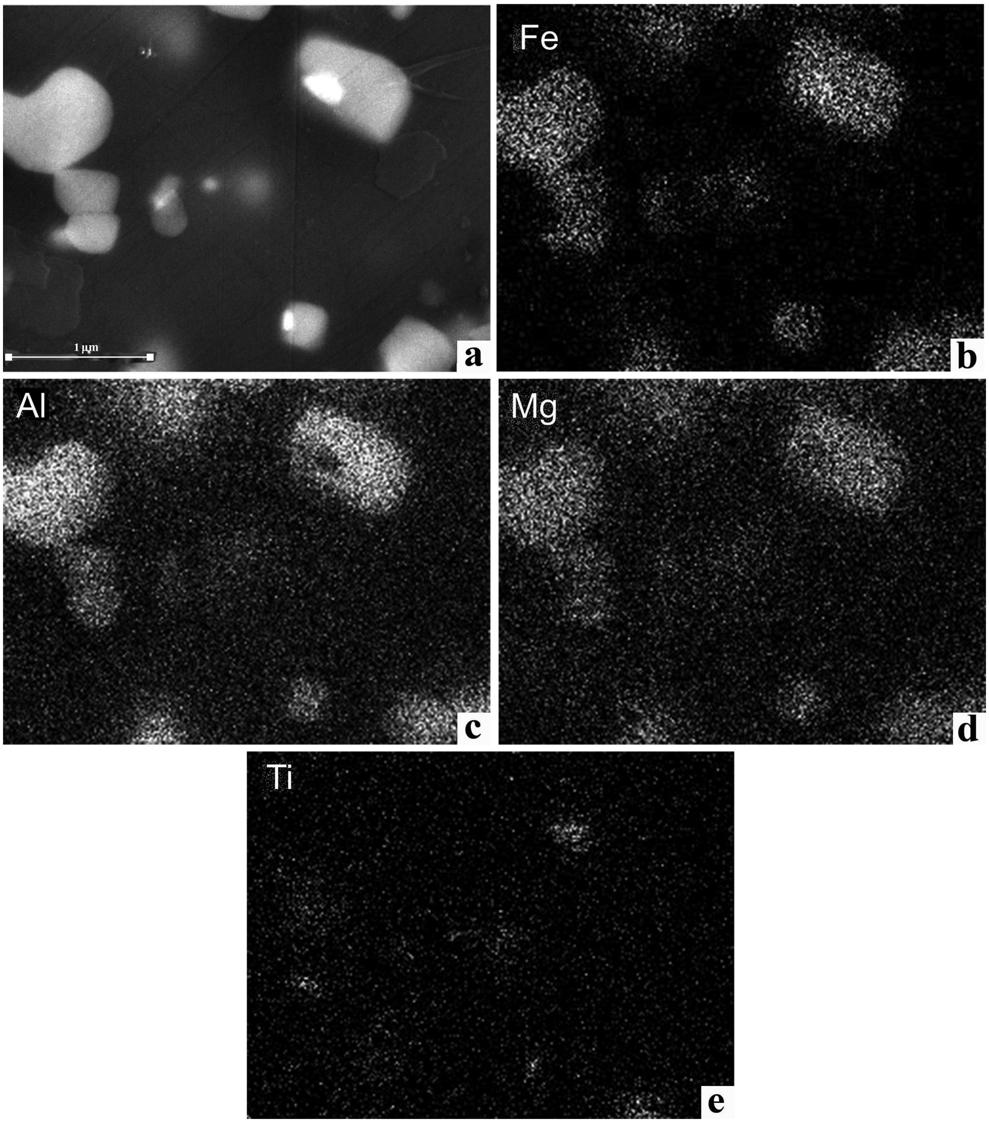

Figure 6. Map of chemical elements distribution in a cluster of fine inclusions in type I tagamites. (a) photomicrograph of the study area and (b)–(e) distributions of chemical elements.

transition and therefore of the presence of magnetite is observed. High-temperature curves reveal the presence of several characteristic points. In about a quarter of samples, a shoulder is observed on heating curves between 130 and 170 °C, which might be linked to iron hydroxides, occurring as films on chalcopyrite grains. Furthermore, Curie temperatures in the 310–430 °C and those in the 510–580 °C range may be associated with fine inclusions which may contain of coexisting magnetite and Al/Ti/Mg-substituted magnetite phases (Fig. 9f).

Low-temperature magnetization curves of type I tagamites are dominated by a strongly magnetic but thermally unstable phase which carries up to 95 per cent of SIRM acquired at 1.8 K. SIRM acquired after ZFC ranges from 0.05 to 0.15 $Am^2\ kg^{-1}$ (with the sole exception of the IS14 sample where it reaches 0.35 $Am^2\ kg^{-1}$) which is roughly two orders of magnitude larger than SIRM acquired at room temperature. FC remanence is always somewhat higher than ZFC, and demagnetizes at higher temperatures, so that the two curves converge between 70 and 150 K depending on the sample. The Verwey transition could not be detected, except for the sample IS14, where it can be seen as a small but discernible minimum in the dM/dT curves centred at 115 K. SIRM acquired at room temperature shows nearly reversible behaviour, SIRM memory approaching 0.94–0.97 (Fig. 10).

In the type II tagamites, low-temperature SIRM demagnetization curves are broadly similar to those for type I, but with a number of notable differences. ZFC SIRM at 1.8 K is somewhat higher than in type I samples, ranging from 0.15 to 0.3 $Am^2\ kg^{-1}$. The phase contributing a major part to remanence acquired at 1.8 K is demagnetized at lower temperatures, below *ca.* 40 K, but the non-demagnetized remainder is considerably larger. The Verwey transition is present in all measured type II samples though in some of them it may be quite weak. Transition temperatures range from 102 to 110 K. Room temperature SIRMs show some irreversibility which generally develops above 100 K. SIRM memory is lower than in type I samples, about 0.7–0.8, in one case reaching 0.87.

Differences in the magnetic behaviour between the two groups of tagamites can be traced in their magnetic hysteresis properties as well. In group I samples, saturation magnetization shows large, over two orders of magnitude, variance, reflecting a considerable difference in the concentration of ferrimagnetic minerals. In a few

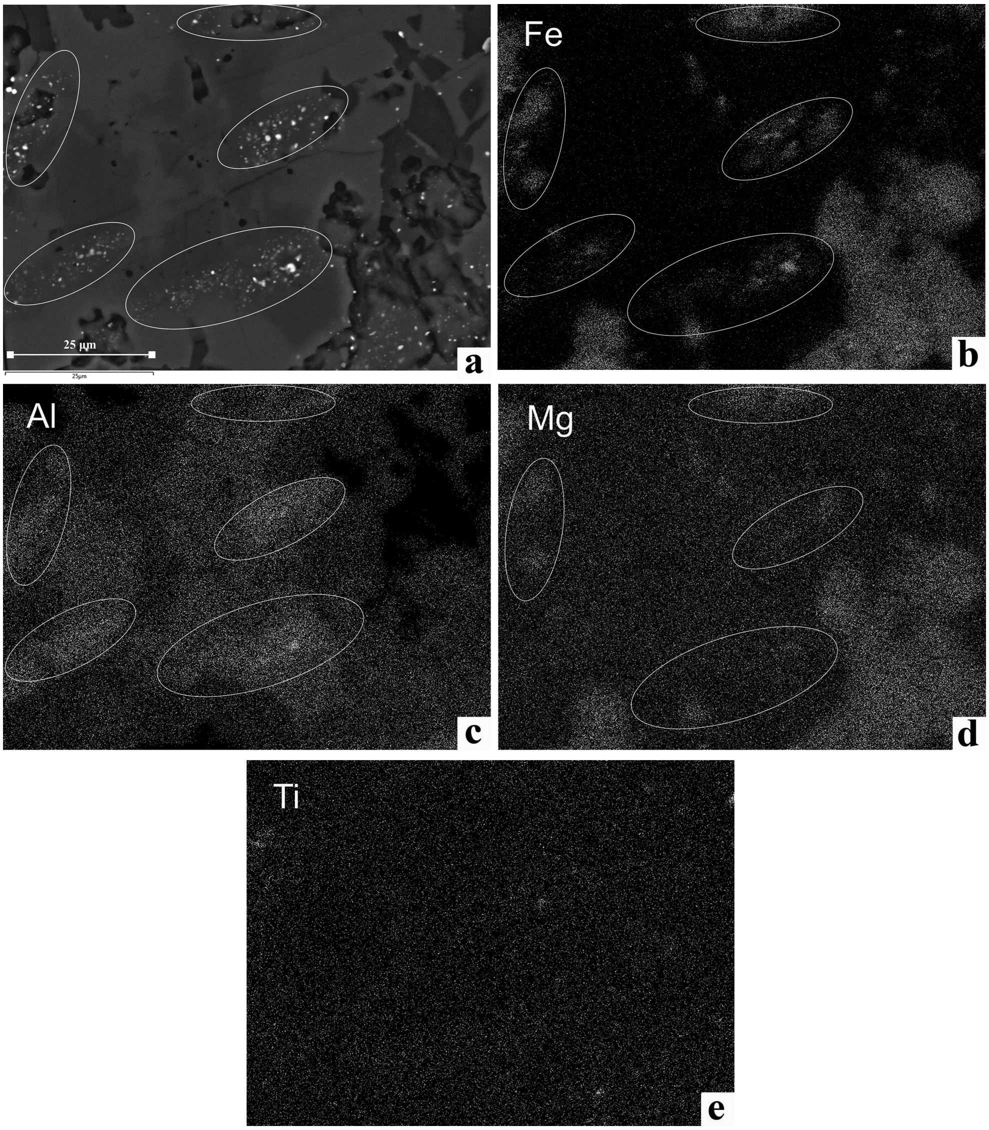

Figure 7. Map of chemical elements distribution in a cluster of fine inclusions in type II tagamites. (a) photomicrograph of the study area and (b)–(e) distributions of chemical elements.

samples with the lowest M_s values, room temperature magnetization versus field curves are dominated by paramagnetic phases. The sample IS14, on the contrary, shows both the highest saturation magnetization and the highest coercivity and M_{rs}/M_s ratio. However, for weakly magnetic samples coercivity and M_{rs}/M_s ratio derived from the loops corrected for high-field slope are somewhat lower than in their more strongly magnetic counterparts. The shape of corrected loops and IRM acquisition curves reveal the presence of a magnetically hard phase not saturated in the 300 mT field (compare e.g. Figs 11a and b). Hysteresis loops in such samples remain open to at least 3 T, while coercivity of remanence seems to be controlled by the hard phase, resulting in a notable scatter of the representative points in the Day plot (Fig. 11f, Day *et al.* 1977).

In most group II samples, saturation magnetization is much higher, and hysteresis loops show an ordinary, ferrimagnetic shape with relatively low M_{rs}/M_s ratio and coercivity (Table 1). In the Day plot, type II tagamites fall into the middle of the pseudo single-domain (PSD) region; their representative points are much more tightly clustered than for type I. However, six samples collected on the same island as type I tagamites (samples IS01-05 and 07) while being quite similar to group II tagamites by their NRM range and thermomagnetic behaviour, and also by microscopic observations, still show somewhat distinct hysteresis properties which place them in an intermediate position between the two groups. Their M_{rs}/M_s ratios and coercivities are in most cases somewhat higher, and the representative points in the Day plot accordingly lie closer to the SD range than for group II proper.

The above difference in the hysteresis behaviour in the two groups of samples becomes much more evident when inspecting their FORC diagrams. For group I samples (Figs 12a–c), FORC distributions show sharp narrow maxima centred at the $H_b = 0$ axis, telltale of (nearly) SD, weakly interacting grains (Roberts *et al.* 2000, 2014). Exact positions of the maxima are somewhat different for the three samples shown, in accordance with their respective bulk coercivities. Group II samples, on the contrary, yield FORC diagrams of a totally different shape (Figs 12e–h). Distribution maxima are rounded, and occur in considerably smaller fields than for group I samples. Outer FORC contours are of onion, rather than triangular, characteristic of the PSD behaviour (Muxworthy & Dunlop 2002; Roberts *et al.* 2014), shape, while FORC general appearance

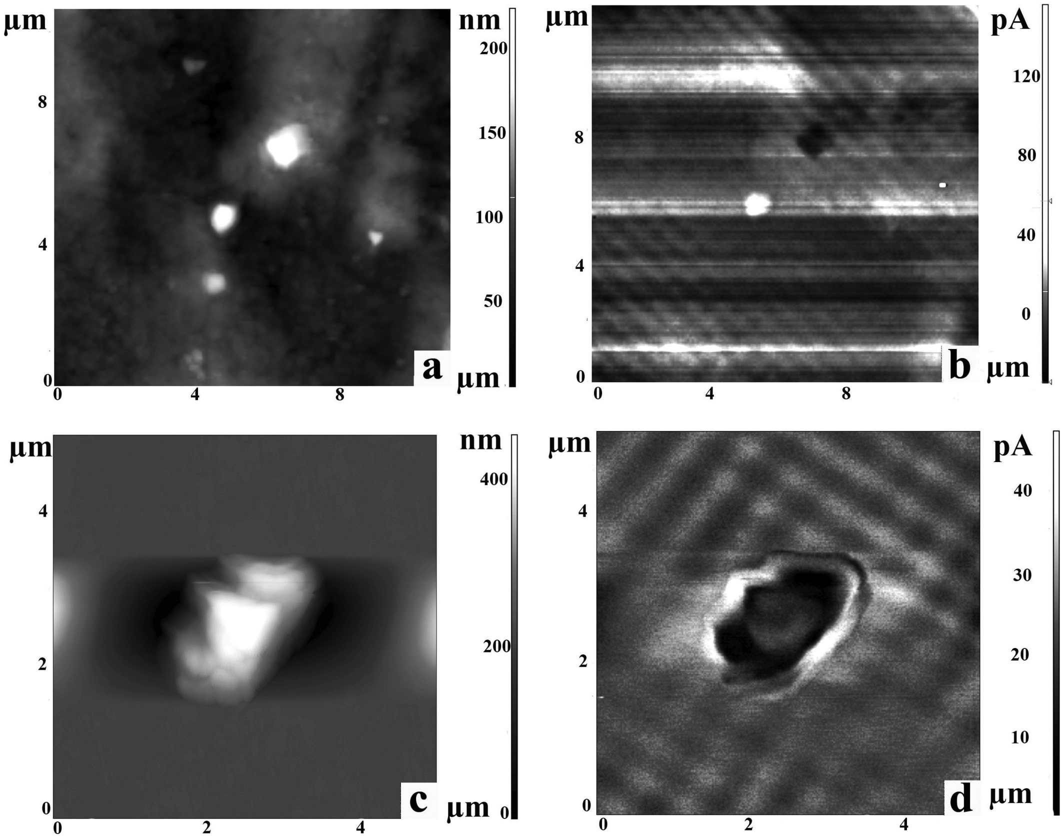

Figure 8. Examples of magnetic force microscopy images of fine inclusions. (a) and (c) surface topography; and (b) and (d) distributions of stray magnetic fields.

resembles that of floppy disks and natural samples containing interacting SD grains (Roberts *et al.* 2000). However, FORC maxima in the latter samples generally occur at considerably higher fields than in ours (25–60 mT against 10–12 mT). We nevertheless posit that the magnetic properties of our group II samples are best described as being due predominantly to an assemblage of strongly interacting, relatively fine particles, rather than by isolated large PSD to MD grains. For the sample IS02, which according to its hysteresis properties belongs to an intermediate group, FORC diagram (Fig. 12d) confirms its position inferred from hysteresis loop characteristics. While the strong central ridge is quite similar to those seen in group I samples, total magnetization appears to contain also a significant contribution from outer onion-like FORC contours.

5 DISCUSSION

The minerals present in tagamites show numerous signs of shock metamorphism, indicating the passage of a strong shock wave with pressure at the front reaching tens of megapascals. High pressure accompanied by very high temperatures (up to several thousand degrees centigrade) produces superheated impact melts that subsequently form impactites body. Several studies of tagamites, for example, from Manicouagan (Floran *et al.* 1978), Mistastin (Grieve 1975), West Clearwater (Phinney *et al.* 1978) impact structures, suggest that cooling of impact melts takes place in two stages (Onorato *et al.* 1978; Simonds *et al.* 1978). At the first stage, the heat of superhot melt with temperature about 2500 °C (Grieve 1975) is consumed to heating and melting of debris, so that the system 'debris-melt' approaches thermal equilibrium. The first stage is characterized by a sharp drop in melt temperature. For fragments with average size 1 mm thermal equilibrium is achieved within 10–100 s (Onorato *et al.* 1978). In most cases, melt temperature drops to and even below crystallization temperatures, that is, melt becomes supercooled. At the second stage, the heat is transferred into the environment, and the melt layer cools as a whole and crystallizes. The second stage of cooling and crystallization of impact melts resembles similar processes in effusive rocks. The two-stage cooling of impact melts naturally produces some specific features in the formed rocks. In the first stage, the main controlling factor is the initial content of debris in melt volume. At the second stage, tagamite structure is influenced primarily by thickness of melt layer, and by the position of a given volume of the melt within the melt layer.

A peculiar feature of Jänisjärvi astrobleme is that impact melt temperature was apparently so high that signatures of shock metamorphism, clearly visible even in suevites, are erased in melt impactites. Most small (first millimetres to first centimetres) target rocks fragments likely experienced pyrogenic melting, either partial or complete. Of the shock metamorphism and melting signatures in quartz inclusions from tagamites, only planar elements (in much smaller amounts than in quartz in the inclusions from suevities) and microperlite jointing (indication of lechatellierite recrystallization) are observed. This indicates a more intense processing of debris by impact melt heat. Depending on the formation conditions, Jänisjärvi tagamites can be classified into two types, reflecting the conditions of the melt cooling. The first type is characterized by an extremely rapid initial cooling of the superheated impact melt. The respective tagamites were crystallized at temperatures above 1200 °C. For type II tagamites, crystallization temperature was significantly lower and the melt enriched with iron. Type I tagamites are further

Table 1. NRM, initial susceptibility, hysteresis parameters and Verwey transition temperatures of the Jänisjärvi tagamites. M_s—saturation magnetization, M_{rs}—saturation remanent magnetization, H_c—coercive force, H_{cr}—remanent coercivity. T_v—Verwey transition temperature, 'none' refers to no transition found in SIRM versus T curves measured with MPMS, dash signifies that no MPMS measurements have been performed. Instrument Codes refer to an instrument used from hysteresis measurements and are as follows: LS—LakeShore Cryotronics VSM 7410, PMC—Princeton Measurements Corporation VSM Model 3900 and MPMS—Quantum Design MPMS 3.

Sample ID	Susceptibility (SI units)	NRM (mA m^{-1})	Mass (mg)	Instrument code	M_s (mA m^2 kg^{-1})	M_{rs} (mA m^2 kg^{-1})	M_{rs}/ M_s	H_c, (mT)	H_{cr} (mT)	H_{cr}/ H_c	T_v (K)
					Type I						
IS 06	–	–	300	PMC	2.64	0.0614	0.023	6.1	37.0	6.12	–
			300	LS	2.70	0.101	0.038	9.5	65.7	6.89	
IS 08	2.44E−04	1.76	34.3	LS	7.89	1.47	0.186	20.5	83.0	4.05	None
			341	PMC	5.18	0.112	0.022	5.5	52.8	9.67	
			34.8	MPMS	3.45	0.307	0.089	11.7	–	–	
IS 09	1.93E−04	2.14	277	LS	3.91	0.567	0.145	21.7	208	9.60	–
IS 10	2.43E−04	13.8	53.5	LS	4.81	0.965	0.201	15.1	–	–	None
			236	PMC	2.23	0.320	0.144	9.8	26.4	2.70	
			53.2	MPMS	3.63	0.811	0.223	12.6	20.5	1.63	
IS 11	2.02E−04	1.45	37.0	LS	1.90	0.336	0.177	14.0	–	–	None
			393	PMC	1.55	0.102	0.066	10.7	56.9	5.30	
			37.0	MPMS	2.22	0.390	0.176	14.3	27.6	1.93	
IS 12	2.74E−04	5.22	176	LS	3.83	0.609	0.159	19.4	38.8	2.00	–
IS 13	3.82E−04	46.3	79.2	LS	8.22	2.53	0.308	13.6	25.7	1.89	None
			371	PMC	4.85	1.65	0.340	14.4	23.9	1.66	
			79.2	MPMS	7.70	2.53	0.328	13.1	22.8	1.74	
IS 14	7.20E−03	17.3	54.5	LS	83.3	31.4	0.376	30.7	62.4	2.03	115
			278	PMC	25.0	8.44	0.337	25.5	46.2	1.81	
			54.5	MPMS	76.2	29.1	0.383	29.7	59.4	2.00	
IS 15	4.47E−04	17.3	182	LS	3.56	0.835	0.235	13.8	31.2	2.26	None
			244	PMC	3.70	0.835	0.226	17.4	37.4	2.15	
			40.2	MPMS	2.34	0.304	0.130	17.1	45.0	2.60	
IS 16	3.47E−04	19.4	235	LS	6.22	1.48	0.239	15.9	30.2	1.90	None
			189	PMC	2.73	0.438	0.160	8.3	26.4	3.19	
			20.7	MPMS	2.55	0.662	0.260	16.4	28.5	1.74	
					Type II						
HS 01	–	–	164	LS	70.0	14.0	0.200	9.4	17.4	1.85	–
HS 02	2.98E−03	124	280	LS	137	19.1	0.140	10.8	27.2	2.52	–
HS 03	2.47E−03	142	223	LS	93.2	12.5	0.134	9.1	21.3	2.34	–
HS 04	1.39E−03	61.4	21.7	LS	60.1	10.2	0.170	9.8	19.1	1.94	108
			271	PMC	33.6	5.80	0.173	10.1	20.1	1.99	
			21.7	MPMS	62.9	10.2	0.162	9.4	18.5	1.97	
HS 05	1.04E−03	50.5	266	LS	33.4	6.60	0.197	10.6	20.7	1.95	–
HS 06	3.40E−03	145	58.5	LS	181	33.1	0.183	13.1	28.5	2.18	107
			172	PMC	176	26.4	0.150	9.8	21.2	2.17	
			58.7	MPMS	181	31.9	0.176	12.3	25.1	2.04	
HS 07	2.78E−03	109	196	LS	44.8	9.49	0.212	11.7	21.8	1.86	–
HS 08	1.86E−03	90.0	32.7	LS	41.8	5.85	0.140	10.6	25.3	2.39	102
			230	PMC	116	14.9	0.129	7.5	17.1	2.29	
			32.9	MPMS	37.6	4.92	0.131	9.2	21.4	2.33	
HS 09	1.58E−03	60.2	436	LS	81.6	11.5	0.141	10.5	24.4	2.32	–
HS 10	2.54E−03	99.4	389	LS	162	20.8	0.128	9.1	21.5	2.38	–
HS 11	2.26E−03	63.0	272	LS	92.1	12.6	0.137	11.8	30.1	2.55	–
HS 12	2.14E−03	80.2	268	LS	184	30.4	0.166	11.1	25.2	2.27	–
HS 13	–	2173	380	LS	82.7	11.9	0.143	9.5	21.4	2.26	–
HS 14	3.78E−03	189.4	266	LS	144	24.3	0.169	10.4	21.7	2.09	–
HS 15	2.93E−03	114	26.6	LS	30.6	7.56	0.247	12.1	22.4	1.85	110
			176	PMC	107	20.4	0.191	10.7	20.5	1.93	
			26.6	MPMS	33.3	8.16	0.245	11.9	21.8	1.83	
HS 16	2.95E−03	356	67.5	LS	105	23.0	0.219	12.3	23.5	1.91	108
			67.8	MPMS	105	21.7	0.207	11.5	21.0	1.83	
					Intermediate samples						
IS 01	1.88E−03	102	211	LS	58.3	14.3	0.244	15.6	32.4	2.08	–
IS 02	1.92E−03	157	246	PMC	65.9	18.4	0.280	16.0	29.7	1.86	–
			292	LS	63.7	17.1	0.269	16.5	32.2	1.95	
IS 03	2.44E−03	104	223	LS	89.3	20.4	0.229	12.8	23.8	1.86	–
IS 04	5.11E−03	248	376	LS	156	23.4	0.150	9.5	25.8	2.72	–
IS 05	4.47E−04	26.4	186	LS	12.7	4.12	0.324	29.8	59.6	2.00	–
IS 07	1.94E−03	138	232	LS	105	32.2	0.306	22.0	50.2	2.28	–

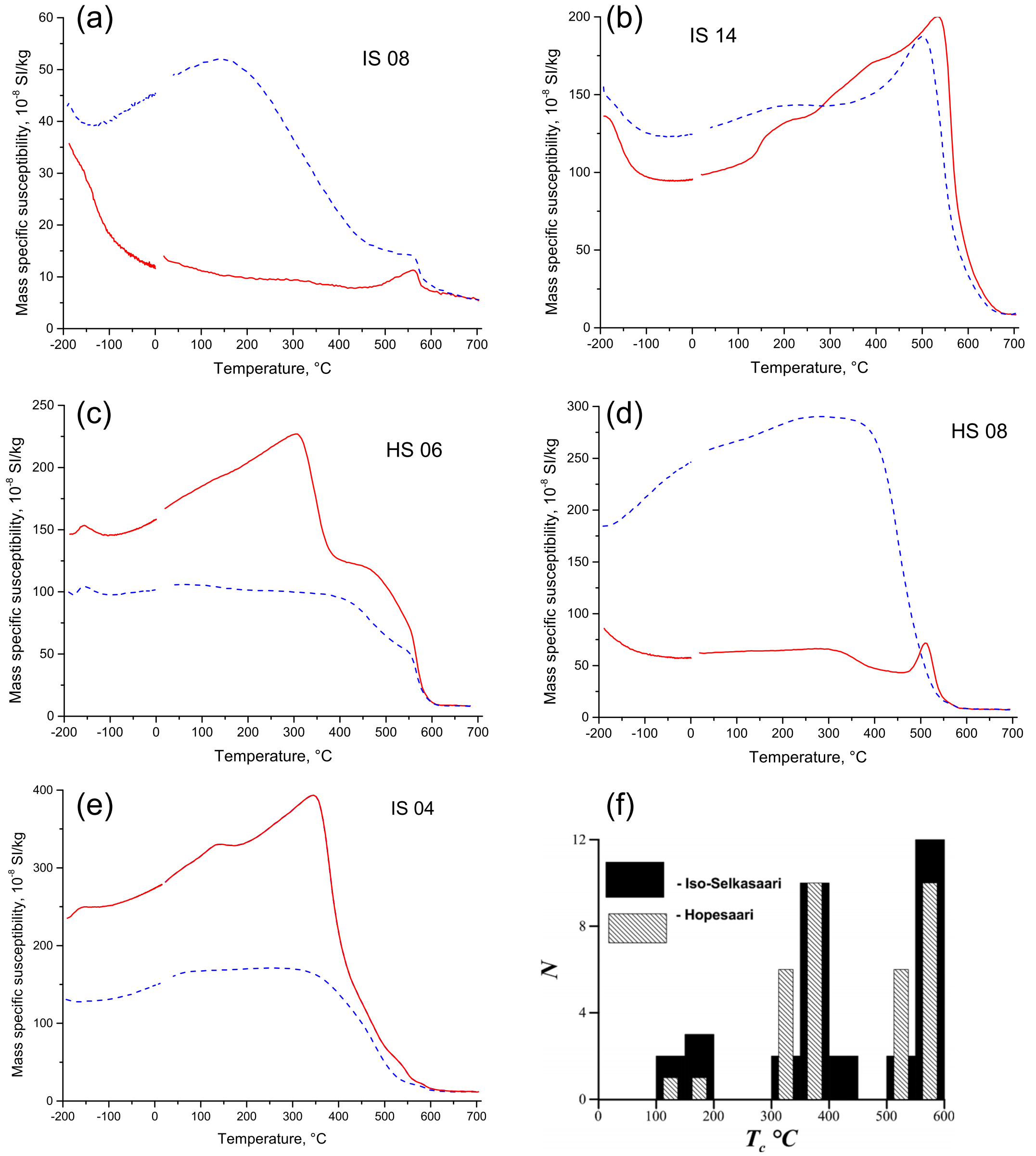

Figure 9. (a)–(e) Temperature dependences of initial magnetic susceptibility and (f) histogram showing the distribution of Curie temperatures. Low-temperature runs on virgin samples and heating curves are shown by solid lines, cooling curves and following low-temperature runs by dashed lines.

characterized by an uneven distribution of large amount of debris fragments accumulated in individual volumes of the melt, which results in a pronouncedly uneven granularity, lower degree of crystallinity and grain uniformity. In both types of impact melts, most iron is bound in the ore minerals, although type II tagamites show also a somewhat higher iron content in cordierite. Overall, this suggests that the crystallization of type I tagamites occurred in strongly non-equilibrium conditions (Sazonova 1984). From the mineralogical point of view, grains of silicate matrix in type I tagamites appear to be coarser. Type I tagamites generally do not contain large isolated grains titanomagnetite which sometimes occur in type II samples.

Both magnetic and microscopic studies confirm that two different types of impact melts were sampled, samples labelled HS01 to IS07 (except for IS06) belonging to type II, with some internal variation in the magnetic properties as discussed above, and samples IS06, IS08 to IS16 to type I, respectively. This is clearly reflected in NRM and initial magnetic susceptibility values. In type I samples, NRM and susceptibility are 1–2 orders of magnitude lower and show much smaller variation than in type II. Titanomagnetite occurs exclusively in type II tagamites as isolated, homogeneous grains about 5–10 μm in size. Its concentration, determined by direct counting of grains in polished sections under a microscope, is less than 0.01 per cent by volume. Titanium content is relatively high, up to 30 per cent TiO_2, which would yield Curie temperatures in the 300–400 °C range and weaker, compared to magnetite, spontaneous magnetization. Areas of increased magnitude of FORC distributions close to the $H_C = 0$ axis seen in FORC diagrams of some group II samples (Figs 12f and g) may be caused by these titanomagnetites which are on average considerably coarser than fine magnetic inclusions in plagioclase. Geological and mineralogical studies of Jänisjärvi impactites (Masaitis *et al.* 1980) show that titanomagnetite develops over secondary minerals, most often enstatite, and should therefore be considered as a secondary mineral itself. Accordingly, its contribution

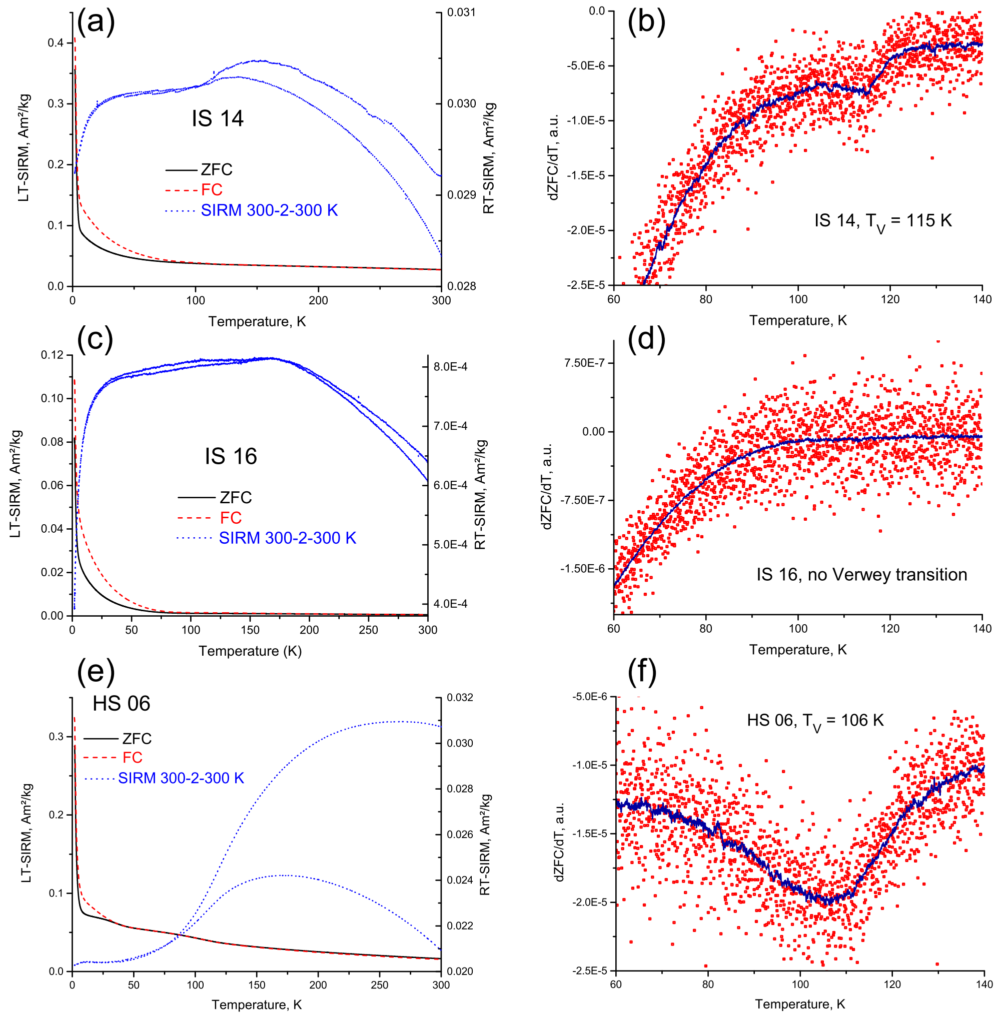

Figure 10. (a), (c) and (e) Low-temperature ZFC and FC SIRM demagnetization and room temperature SIRM cycling from 300 to 2 K and back in zero field and (b), (d) and (f) temperature derivatives of ZFC SIRM versus temperature curves showing presence or absence of the Verwey transition.

to NRM while significant in some cases, postdates the impact event by an unclear amount of time.

Fine inclusions of ore minerals occur as small (1–2 µm and less, down to 50–100 nm) grains either clustered (type II) or uniformly distributed (type I) in non-magnetic (silicate) matrix. Clusters are most common in plagioclase. Concentration of fine inclusions within clusters, determined with an open source analysis and processing software ImageJ (http://imagej.net), reaches 1–5 per cent (in rare cases up to 10 per cent), while their total volume concentration in the rock is generally $\leq$ 1 per cent. Microscopic studies suggest that individual grains of fine inclusions are chemically heterogeneous, often consisting of at least two different phases. The first phase occupying generally <20 per cent of the grain volume contain only minor titanium impurities (<4 per cent) and can be assumed to be fairly close to magnetite. The second phase contains significant amounts of Ti and Al impurities (up to 40 per cent) and up to 10 per cent Mg.

Magnetic force microscopy (Figs 8b and d) shows that fine inclusions may be strongly magnetic. To evaluate whether inclusions and their clusters alone can explain the observed magnetic properties of Jänisjärvi tagamites, we employed a model treating a sample as an ensemble of interacting particles (Kharitonskii *et al.* 2016). In the framework of this model, clusters are considered as ensembles of magnetostatically interacting SD particles with the 'effective' (averaged over the volume of two-phase particles) spontaneous magnetization. Let α and β be the relative number of magnetic moments oriented parallel or antiparallel to the direction of a reference axis, respectively. Then the magnetization ζ of a cluster in an external field H directed along a reference axis is calculated as follows:

$$\zeta = \alpha - \beta = I/(\eta\, I_s) = \int_{-H_0}^{\infty} W(H_i - H)\, dH_i - \int_{-\infty}^{-H_0} W(H_i - H)\, dH_i, \qquad (1)$$

where I_s–particle saturation magnetization, I–magnetization of a cluster in the field H, η–concentration of ferromagnetic particles in a cluster and H_0–critical field of magnetization reversal. Function $W(H_i)$ has the meaning of density distribution of dipole–dipole interaction fields within the cluster, which in the local field approximation can be obtained using the modified moments method (Al'miev *et al.* 1994).

We consider primarily the type I tagamites where fine inclusions appear to be the sole NRM carrier. Furthermore, from microscopic observations they are relatively uniformly distributed in a non-magnetic matrix and can computationally be treated as a single cluster. To find possible values of effective spontaneous magnetization, we solve numerically an inverse problem comparing

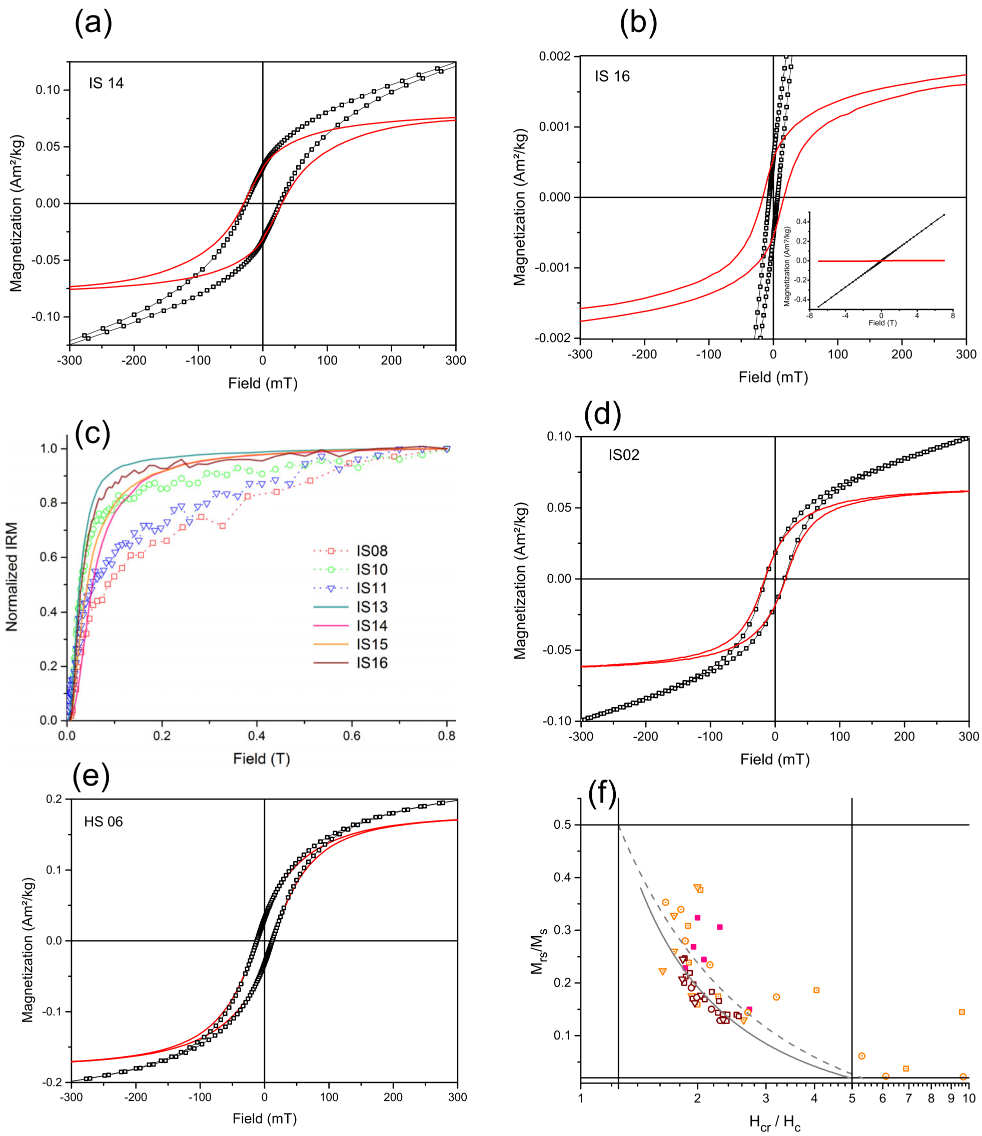

Figure 11. (a), (b), (d) and (e) Central parts of raw (open squares) and corrected for paramagnetism (solid lines) hysteresis loops. Loops in (a), (b) and (d) were measured with an MPMS 3 instrument in a maximum field 7 T, loop in (e) with a PMC VSM 3900 in a maximum field 1.5 T. The inset in (b) shows the full 7 T loop demonstrating dominance of the paramagnetic contribution to the total magnetization signal. (c) IRM acquisition curves for representative samples of group I tagamites. All curves were normalized to the respective maximum IRM values. (f) Day plot summarizing all measured hysteresis data. Light colour open symbols—group I, dark open symbols—group II, solid symbols—'intermediate' samples (see the text). Symbol shape codes measurements made with different instruments: squares—LS VSM 7410, circles—PMC VSM 3900 and triangles—MPMS 3. Lines show two SD-MD mixing models by Dunlop (2002).

experimental values of saturation magnetization I_s with the values obtained from formula (1). Varying the concentration η between 10^{-3} and 10^{-4} (the range compatible with microscopic observations), we obtain the effective spontaneous magnetization values ranging from about 30 to 400 kA m^{-1}, depending on a sample. The latter value is compatible with a near-magnetite phase found in most strongly magnetic type I samples such as IS14. The former, while still too high for a magnetically hard phase like hematite or goethite, may correspond instead to two-phase particles as inferred from microscopic observations. An individual fine inclusion can thus be viewed as a system of two regions with substantially different chemical composition whose spontaneous magnetizations differ by at least 1–2 orders of magnitude. This estimate confirms therefore that fine inclusions, as well as clusters thereof (in type II samples), contribute significantly to the tagamites NRM. Within clusters, magnetic grains are bound by magnetostatic interaction, as attested by FORC diagrams (Figs 12e–h).

Observed differences in the magnetic properties of the samples from two sampling sites might be caused by their belonging to different geological and/or morphological regions, as well as differences in magnetic mineralogy, which in turn may indicate the temperature of minerals crystallization. By their petrographic and geochemical features, tagamites can be viewed as a continuous series between the two extrema: high temperature (HT-tg), formed from the impact melt at temperatures >2000 °C, and low temperature (LT-tg), when the melt temperature is only slightly above the melting point of a rock. Hallmarks of the extreme members are NRM value which is 1–2 orders of magnitude lower for HT-tg than for LT-tg, and magnetic domain state. The room temperature magnetic responce of HT tagamites (type I) is dominated by weakly interacting SD particles. However, type I samples contain also a significant amount of a magnetically hard phase which in the weakest samples may account for up to one-third of room temperature SIRM (Fig. 11c). These samples also show a superparamagnetic-like behaviour at low

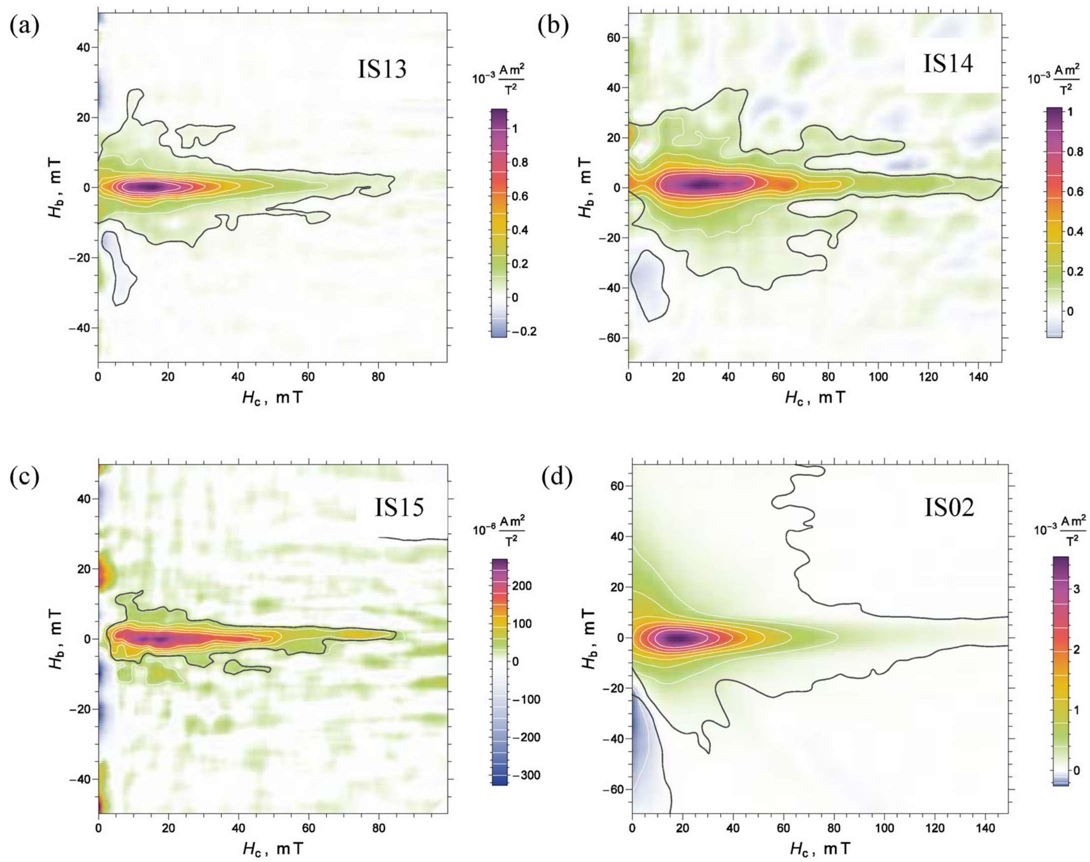

Figure 12. FORC diagrams for eight representative samples. (a)–(c) group I, (d) an intermediate sample, (e)–(h) group II. All FORC distributions have been computed with the VARIFORC software (Egli 2013) using variable smoothing with initial smoothing factor of 4 and SF increase coefficient λ of 0.07 in both horizontal and vertical directions. Note that field limits in (a) and (d) are different from those in the other panels. Grey lines show contours corresponding to signal-to-noise ratios of 3.

temperatures (e.g. Figs 10a and c). The mineralogy of this phase is difficult to establish with certainty but its behaviour resembles closely that of various nano-sized iron hydroxides such as goethite (Banerjee 2006), lepidocrocite (Hirt *et al.* 2002; Till *et al.* 2014), or ferrihydrite (Guyodo *et al.* 2006). LT tagamites (type II), on the other hand, contain a mixture of strongly interacting SD and MD particles. This is consistent with the observed composition of ilmenite, which is expected to be more uniform in composition and poorer in trace elements when formed from a hot melt with low content of target debris. Conversely, if tagamites are formed from a melt with high initial content of target debris, ilmenite shows an inhomogeneous composition and becomes increasingly enriched in trace elements. In Jänisjärvi samples, the content of impurities (Al_2O_3, MgO and Cr_2O_3) in ilmenite is small, on average less than 1 per cent, and down to their complete absence (Sazonova & Kononkova 1988). Besides, in ilmenite from impacted shale target (impact pressure of 13–25 GPa) rutile lamellae are observed, amount of rutile growing with the increase of impact pressure. Such formation conditions favour a very fast crystallization of fine inclusions of ore minerals with cooling of the melt. The latter would likely retain their structural, chemical and magnetic state unchanged. We argue therefore that remanence carried by fine inclusions is primary (i.e. cogenetic to the impact). Its further palaeomagnetic stability, however, would depend on the prevailing magnetic domain state. It might be expected therefore that in type I tagamites NRM would be reasonably stable, while in type II samples NRM may be prone to alteration because of lessened magnetic stability of strongly interacting grains.

6 CONCLUSIONS

1. Jänisjärvi tagamites are represented by two genetic varieties. High-temperature type I tagamites were formed from impact melt at above 2000 °C and quickly crystallized at temperatures above 1200 °C. Type II tagamites, low-temperature, were crystallized from more iron-enriched melt and at a considerably slower cooling rate. Formation conditions may result in the crystallization of fine metal-enriched inclusions within plagioclase matrix starting from the earliest stages of melt cooling in both types of tagamites.

2. Inclusions in both types of tagamites are small (tens of nanometres to few micrometres) chemically and magnetically inhomogeneous particles. In type I tagamites, magnetostatic interaction between individual inclusions is weak, while inclusions themselves may be viewed as consisting of coexistent strongly and weakly magnetic regions. In type II tagamites, inclusions are rather tightly clustered within plagioclase grains and bound with strong magnetostatic interaction.

3. Fine magnetic inclusions are embedded in the matrix of a weakly metamorphosed rock and, apparently, did not experience any significant physical and chemical changes after crystallization, likely retaining their structural, chemical and magnetic state.

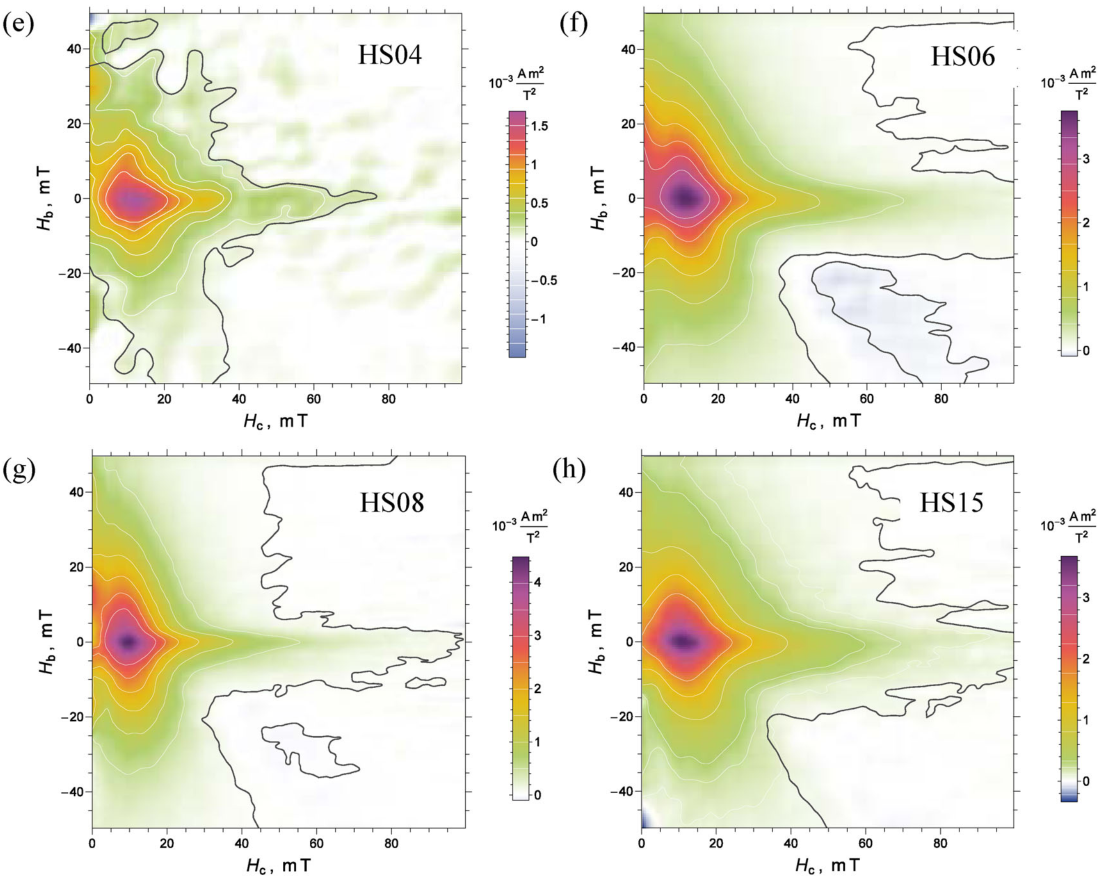

Figure 12 (*continued.*)

Remanent magnetization of inclusions is likely acquired at the time of crystallization and can therefore carry information about the geomagnetic field immediately after the impact event. However, strong magnetostatic interaction between inclusions, as seen in type II tagamites, may adversely affect their palaeomagnetic stability.

ACKNOWLEDGEMENTS

Sampling at the Jänisjärvi astrobleme has been supported by St. Petersburg State University (project 11.42.1314.2014 Expedition for geophysical studies in the northwest region of Russia). We thank Svyatoslav Sokolov (Petrozavodsk State University) for acquainting us with impactites outcrops at Jänisjärvi Lake, and Radmila Smirnova, Vladimir Karpinskii and Andrey Yakubson for the assistance during fieldwork and sampling. Scientific research was carried out using the facilities of the Research Park of St. Petersburg State University at: Center for Diagnostics of Functional Materials for Medicine, Pharmacology and Nanoelectronics, Center for Nanofabrication of Photoactive Materials (Nanophotonics), Interdisciplinary Center for Nanotechnology, Center for Geo-Environmental Research and Modeling (GEOMODEL), Center for Microscopy and Microanalysis and Center for Innovative Technologies of Composite Nanomaterials. We thank Svetlana Yanson, Vladimir Mikhailovskii, Natalia Vlasenko, Vladimir Shilovskikh for help with optical and SEM observations, Maxim Lozhkin for MFM observations, Evgenii Shevchenko, Alexandr Sakhatskii and Denis Nazarov for magnetic measurements. Some magnetic measurements have been made at the Laboratory of the Main Geomagnetic Field and Petromagnetism (Institute of Physics of the Earth RAS, Moscow). We thank Vladimir Pavlov for arranging a visit of one of us (AK) to the laboratory, and Roman Veselovskii for help with measurements. This paper has benefited from the reviews by Mike Jackson and an anonymous reviewer.

REFERENCES

Al'miev, A.S., Ralin, A. Yu. & Kharitonskii, P.V., 1994. Distribution functions of dipole-dipole interaction fields in dilute magnetic materials, *Phys. Met. Metallogr.,* **78,** 28–34.

Banerjee, S.K., 2006. Environmental magnetism of nanophase iron minerals: testing the biomineralization pathway, *Phys. Earth planet. Inter.,* **154,** 210–221.

Carporzen, L., Gilder, S.A. & Hart, R.J., 2005. Palaeomagnetism of the Vredefort meteorite crater and implications for craters on Mars, *Nature,* **435,** 198–201.

Cloete, M., Hart, R.J., Schmid, H.K., Drury, M., Demanet, C.M. & Sankar, K.V., 1999. Characterization of magnetite particles in shocked quartz by means of electron- and magnetic force microscopy: Vredefort, South Africa, *Contrib. Mineral. Petrol.,* **137,** 232–245.

Day, R., Fuller, M.D. & Schmidt, V.A., 1977. Hysteresis properties of titanomagnetites: grain size and composition dependence, *Phys. Earth planet. Inter.,* **13,** 260–267.

Dence, M.R., 1971. Impact melts, *J. geophys. Res.,* **76,** 5552–5565.

Dressler, B.O. & Reimold, W.U., 2001. Terrestrial impact melt rocks and glasses, *Earth-Sci. Rev.,* **56,** 205–284.

Dunlop, D.J., 2002. Theory and application of the Day plot (M_{rs}/M_s versus H_{cr}/H_c), 1. Theoretical curves and tests using titanomagnetite data, *J. geophys. Res.,* **107,** doi:10.1029/2001JB000486.

Egli, R., 2013. VARIFORC: an optimized protocol for calculating non-regular first-order reversal curve (FORC) diagrams, *Glob. Planet. Change,* **110,** 302–320.

Eitel, M., Gilder, S.A., Kunzmann, T. & Pohl, J., 2014. Rochechouart impact crater melt breccias record no geomagnetic field reversal, *Earth planet. Sci. Lett.,* **387,** 97–106.

Eitel, M., Gilder, S.A., Spray, J., Thompson, L. & Pohl, J., 2016. A paleomagnetic and rock magnetic study of the Manicouagan impact structure: implications for crater formation and geodynamo effects, *J. geophys. Res.,* **121,** 436–454.

Elming, S.A. & Bylund, G., 1991. Paleomagnetism and the Siljan impact structure, central Sweden, *Geophys. J. Int.,* **105,** 757–770.

Elmore, R.D. & Dulin, S., 2007. New paleomagnetic age constraints on the Decaturville impact structure and Weaubleau structure along the 38th parallel in Missouri (North America), *Geophys. Res. Lett.,* **34,** L13308, doi:10.1029/2007GL030113.

Elo, S., Zhdanova, L., Chepik, A., Pesonen, L.J., Philippov, N. & Shelemotov, A., 2000. Comparative geophysical description and modelling of Lappajärvi and Jänisjärvi structures, Fennoscandian Shield (abstract), in *Meteorite Impacts Precambrian Shields: Programme and Abstracts, 4th Workshop of the European Science Foundation Impact Programme,* , p. 35.

Fairchild, L.M., Swanson-Hysell, N.L. & Tikoo, S.M., 2016. A matter of minutes: breccia dike paleomagnetism provides evidence for rapid crater modification, *Geology,* **44,** 723–726.

Fel'dman, V.I., Sazonova, L.V. & Granovsky, L.B., 1982. A classification of impactites based on petrographic and geological features (in Russian), *Bull. MOIP Otdel. Geol.,* **57,** 84–94.

Floran, R.J., Grieve, R.A.F., Phinney, W.G., Warner, J.L., Simonds, C.H., Blanchard, D.P. & Dence, H.R., 1978. Manicouagan impact melt, Quebec. Stratigraphy, petrology and chemistry, *J. geophys. Res.,* **83,** 2737–2759.

Gibson, R.L., Reimold, W.U., Ashley, A.J. & Koeberl, C., 2001. Shock pressure distribution in the Vredefort impact structure, South Africa: evidence from feldspar and ferromagnesian minerals, in *32nd Annual Lunar and Planetary Science Conference*, March 12–16, 2001, Houston, Texas, abstract no. 1012.

Grieve, R.A.F., 1975. Petrology and chemistry of the impact melt at Mistastin Lake crater, Labrador, *Bull. geol. Soc. Am*., **86,** 1617–1629.

Guyodo, Y., Banerjee, S.K., Penn, R.L., Burleson, D., Berquo, T.S., Seda, T. & Solheid, P., 2006. Magnetic properties of synthetic six-line ferrihydrite nanoparticles, *Phys. Earth planet. Inter.,* **154,** 222–233.

Halls, H.C., 2009. A 100 km-long paleomagnetic traverse radial to the Sudbury Structure, Canada and its bearing on Proterozoic deformation and metamorphism of the surrounding basement, *Tectonophysics,* **474,** 493–506.

Henkel, H. & Reimold, W.U., 2002. Magnetic model of the central uplift of the Vredefort impact structure, South Africa, *J. appl. Geophys.,* **51,** 43–62.

Hervé, G., Gilder, S.A., Marion, C.L., Osinski, G.R., Pohl, J., Petersen, N. & Sylvester, P.J., 2015. Paleomagnetic and rock magnetic study of the Mistastin Lake impact structure (Labrador, Canada): implications for geomagnetic perturbation and shock effects, *Earth planet. Sci. Lett.,* **417,** 151–163.

Hirt, A.M., Lanci, L., Dobson, J., Weidler, P. & Gehring, A.U., 2002. Low-temperature magnetic properties of lepidocrocite, *J. geophys. Res.,* **107,** doi:10.1029/2001JB000242.

Jourdan, F., Renne, P.R. & Reimold, W.U., 2008. High-precision $^{40}Ar/^{39}Ar$ age of the Jänisjärvi impact structure (Russia), *Earth planet. Sci. Lett.,* **265,** 438–449.

Kharitonskii, P.V., Gareev, K.G., Frolov, A.M., Lebedev, S.V. & Velikorussov, P.V., 2016. The investigation of superparamagnetic colloidal particles Fe_3O_4–SiO_2, *Solid State Phenom.,* **247,** 138–141.

Koch, S.A., Gilder, S.A., Pohl, J. & Trepmann, C., 2012. Geomagnetic field intensity recorded after impact in the Ries meteorite crater, Germany, *Geophys. J. Int.,* **189,** 383–390.

Louzada, K.L., Weiss, B.P., Maloof, A.C., Stewart, S.T., Swanson-Hysell, N. & Soule, S.A., 2008. Paleomagnetism of Lonar Crater, India, *Earth planet. Sci. Lett.,* **275,** 308–319.

Masaitis, V.L., Sindeev, A.S. & Staritsky, Yu. G., 1976. The impactites of the Jänisjärvi astrobleme (in Russian), *Meteoritika,* **35,** 103–110.

Masaitis, V.L., Danilin, A.N., Mashchak, M.S., Raykhlin, A.I., Selivanovskaya, T.V. & Shadenkov, Ye. M., 1980. *The Geology of Astroblemes,* Leningrad, Nedra (in Russian).

Muxworthy, A.R. & Dunlop, D.J., 2002. First-order reversal curve (FORC) diagrams for pseudo-single-domain magnetites at high temperature, *Earth planet. Sci. Lett.,* **203,** 369–382.

Onorato, P.J. K., Uhlmann, D.R. & Simonds, C.H., 1978. The thermal history of the Manicouagan impact melt sheet, Quebec, *J. geophys. Res.,* **83,** 2789–2798.

Pesonen, L.J., Marcos, N. & Pipping, F., 1992. Paleomagnetism of the Lappajärvi impact structure, western Finland, *Tectonophysics,* **216,** 123–142.

Phinney, W.C., Simonds, C.H., Cochran, A. & McGee, P.E., 1978. West Clearwater, Quebec impact structure, Part II: Petrology, in *Proceedings of the 9th Lunar and Planetary Science Conference,* Vol. 2, pp. 2659–2693.

Pilkington, M., Ames, D.E. & Hildebrand, A.R., 2004. Magnetic mineralogy of the Yaxcopoil-1 core, Chicxulub, *Meteorit. Planet. Sci.,* **39,** 831–841.

Plado, J., Pesonen, L.J., Koeberl, C. & Elo, S., 2000. The Bosumtwi meteorite impact structure, Ghana: a magnetic model, *Meteorit. Planet. Sci.,* **35,** 723–732.

Poornachandra Rao, G.V.S. & Bhalla, M.S., 1984. Lonar Lake: palaeomagnetic evidence of shock origin, *Geophys. J. R. astr. Soc.,* **77,** 847–862.

Raiskila, S., Salminen, J., Elbra, T. & Pesonen, L.J., 2011. Rock magnetic and paleomagnetic study of the Keurusselkä impact structure, central Finland, *Meteorit. Planet. Sci.,* **46,** 1670–1687.

Riller, U., 2005. Structural characteristics of the Sudbury impact structure, Canada: impact-induced versus orogenic deformation–a review, *Meteorit. Planet. Sci.,* **40,** 1723–1740.

Roberts, A.P., Pike, C.R. & Verosub, K.L., 2000. First-order reversal curve diagrams: a new tool for characterizing the magnetic properties of natural samples, *J. geophys. Res.,* **105,** 28 461–28 475.

Roberts, A.P., Heslop, D., Zhao, X. & Pike, C.R., 2014. Understanding fine magnetic particle systems through use of first-order reversal curve diagrams, *Rev. Geophys.,* **52,** 557–602.

Rochette, P., Gattacceca, J., Devouard, B., Moustard, F., Bezaeva, N.S., Cournède, C. & Scaillet, B., 2015. Magnetic properties of tektites and other related impact glasses, *Earth planet. Sci. Lett.,* **432,** 381–390.

Salminen, J.M., Donadini, F., Pesonen, L.J., Masaitis, V.L. & Naumov, M.V., 2006. Paleomagnetism and petrophysics of the Jänisjärvi impact structure, Russian Karelia, *Meteorit. Planet. Sci.,* **41,** 1853–1870.

Sazonova, L.V. & Kononkova, N.N., 1988. Ilmenite in impactites of Jänisjärvi astrobleme (in Russian), *Mineral. J.,* **10,** 28–35.

Sazonova, L.V., 1984. *Petrography of impactites of Jänisjärvi astrobleme, PhD thesis*, Moscow, Moscow State University (in Russian).

Schmidt, P.W. & Williams, G.E., 1991. Paleomagnetic correlation of the Acraman impact structure and the late Proterozoic Bunyeroo ejecta horizon, South Australia, *Aust. J. Earth Sci.,* **38,** 283–289.

Schmidt, P.W. & Williams, G.E., 1996. Palaeomagnetism of the ejecta-bearing Bunyeroo Formation, late Neoproterozic, Adelaide fold belt, and the age of the Acraman impact, *Earth planet. Sci. Lett.,* **144,** 347–357.

Simonds, G.H., Floran, P.J., McGee, P.E., Phinney, W.C. & Yarner, J.L., 1978. Petrogenesis of melt rocks, Manicouagan impact crater, Quebec, *J. geophys. Res.,* **83,** 2773–2788.

Steiner, M.B., 1996. Implications of magneto-mineralogic characteristics of the Manson and Chicxulub impact rocks, *Geol. Soc. Am. Spec. Pap.,* **307,** 89–104.

Till, J.L., Guyodo, Y., Lagroix, F., Ona-Nguema, G. & Brest, J., 2014. Magnetic comparison of abiogenic and biogenic alteration products of lepidocrocite, *Earth planet. Sci. Lett.,* **395,** 149–158.

Zhdanov, V.V. *et al.*, 2009. Impact (coptogenic) rock-assemblages, in *Petrographic Code of Russia: Magmatic, Metamorphic, Metasomatic and Impact Formations,* pp. 79–85, eds Bogatikov, O.A., Petrov, O.V. & Morozov, A.F., VSEGEI Press.